



## ORIGINAL ARTICLE

# Structural analysis and immunomodulatory activity of a homopolysaccharide isolated from *Parabacteroides distasonis*



Yanglu Zhu<sup>a</sup>, Ying Cai<sup>a</sup>, Xueqin Cao<sup>a</sup>, Pei Li<sup>b</sup>, Deliang Liu<sup>a</sup>, Simin Ye<sup>a</sup>, Zengmei Xu<sup>a</sup>, Baochun Shen<sup>c</sup>, Qiongfeng Liao<sup>b,\*</sup>, Hao Li<sup>a,\*</sup>, Zhiyong Xie<sup>a,\*</sup>

<sup>a</sup> School of Pharmaceutical Sciences (Shenzhen), Sun Yat-sen University, Guangzhou 510006, PR China

<sup>b</sup> School of Pharmaceutical Sciences, Guangzhou University of Chinese Medicine, Guangzhou 510006, PR China

<sup>c</sup> School of Pharmacy, Kunming Medical University, Kunming 650500, PR China

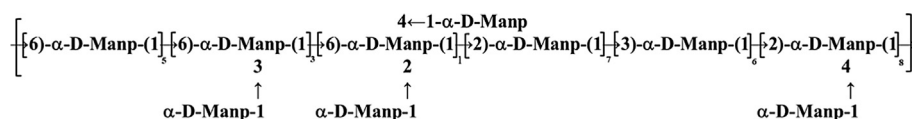
Received 11 December 2021; accepted 30 January 2022

Available online 3 February 2022

## KEYWORDS

Exopolysaccharide;  
*Parabacteroides distasonis*;  
Structural characterization;  
Immunomodulatory activity

**Abstract** A homopolysaccharide fraction (PEP-1A) with desired immunomodulatory activity was isolated from culture broth of *Parabacteroides distasonis*. Structural characterization uncovered that PEP-1A had a molecular weight of  $3.40 \times 10^6$  Da and possessed mannose merely. Comprehensive analysis of FT-IR, GC-MS and 1D/2D NMR confirmed that the structure of PEP-1A was expected as follows:



Finally, the activity assays on RAW 264.7 macrophages showed that PEP-1A could promote proliferation, increase the production of reactive oxygen species (ROS), enhance the phagocytosis, and promote the secretion of nitric oxide (NO) and inflammatory cytokines including IL-1 $\beta$ , IL-6 and TNF- $\alpha$ . Furthermore, PEP-1A could give play to immunoregulation effect through NF- $\kappa$ B, MAPK and Akt signaling pathways. Collectively, the study of PEP-1A offers a molecular underpinning for the future application of PEP-1A as a potential immunostimulant.

© 2022 The Authors. Published by Elsevier B.V. on behalf of King Saud University. This is an open access article under the CC BY-NC-ND license (<http://creativecommons.org/licenses/by-nc-nd/4.0/>).

\* Corresponding authors.

E-mail addresses: zyxiao@gzucm.edu.cn (Q. Liao), lihao258@mail.sysu.edu.cn (H. Li), xiezhy@mail.sysu.edu.cn (Z. Xie).

Peer review under responsibility of King Saud University.



## 1. Introduction

Compared with plant polysaccharides and animal polysaccharides, exopolysaccharides (EPS) have attracted the attention of many researchers due to short production cycle, easy control of production conditions, relatively stable yield and quality, and less influence by geography and climate. EPS are long chain polymer compounds secreted into extracellular broth or closely connected with cells by microorganism during metabolism (Hidalgo-Cantabrana et al., 2014). As a kind of non-toxic biological macromolecules, EPS have attracted more and more attention due to its antitumor (Farang et al., 2020), antioxidative (Guo et al., 2010), immunomodulatory (Wang et al., 2020), hypoglycemic (Sun et al., 2021) and other admirable biological activities. Among these, most effects of polysaccharides are thought to be due to the regulation of innate immunity, and more specifically, the function of macrophages (Schepetkin and Quinn, 2006). The innate immune response is the first obstacle to resist pathogens invasion and foreign substances, where cells like macrophages, not only play a defined role in major responses to pathogens, but also exert a vital function on the coordination of tissue homeostasis, adaptive immune response. Moreover, relevant studies have shown that enhancing the immune system has a good therapeutic effect on diseases such as immunosuppression, microbial infection and malignant tumor (Hotchkiss RS and Monneret G, 2013).

Microorganisms, especially bioactive bacteria, have attracted extensive attention due to their ability to produce EPS that may be related to their probiotic activities. To date, studies on bacterial EPS were concerned about lactic acid bacteria, but took little interest in other bacteria with probiotic activities, especially intestinal bacteria, moreover, most studies on bacterial EPS had tended to elucidate the preliminary analysis of molecular weight and monosaccharide composition, and lost sight of their detailed structure (Hu et al., 2021; Jiang et al., 2020; Zhao et al., 2021). *Parabacteroides distasonis* (*P. distasonis*), a gram-negative and strictly anaerobic gut bacterium, has received increasing research attention due to its various probiotic activities on attenuating obesity (K. Wang et al., 2019), colitis (Dziarski et al., 2016), multiple sclerosis (Cekanaviciute et al., 2017) and colon tumor (Koh et al., 2021). However, existing studies on *P. distasonis* mainly focused on its live status and related membrane substances. As an important active component of *P. distasonis*, few writers have been able to draw systematic research into the characterization and biological activities of purified EPS secreted by *P. distasonis*, which is detrimental to the subsequent application and development.

In this study, we isolated and purified a mannan EPS from *P. distasonis*, analyzed its possible structure in virtue of FT-IR, HPLC, GC-MS, and 1D/2D NMR. Its immunoregulatory activity was also explored on RAW 264.7 macrophages. We found that NF- $\kappa$ B, MAPK, and Akt signaling pathways may play a vital role in activation of PEP-1A-stimulated macrophages, subsequently leading to a cascade of reactions, including promoting the production of ROS and NO, inducing the release of cytokines and enhancing the phagocytosis. This is the first study reporting a mannan homopolysaccharide from *P. distasonis* to be structurally characterized and its immunomodulatory activity clarified. The study not only lays a foundation for future application of PEP-1A but also

expands the application value of *P. distasonis*. This research will provide a vital opportunity to advance the understanding of EPS and further make contributions in interpreting the therapeutic effect of gut microbiota when ameliorating diseases.

## 2. Materials and methods

### 2.1. Materials and chemicals

*P. distasonis* ATCC 8503 and RAW 264.7 cells were purchased from American Type Culture Collection (ATCC). DEAE Cellulose DE-52, neutral red, polymyxin B (PMB), 3-(4,5-Dimethylthiazol-2-yl)-2,5-diphenyl-tetrazolium bromide (MTT) were purchased from Beijing Solarbio Science and Technology Co. Ltd. (Beijing, China). Lipopolysaccharide (LPS) and monosaccharide standards were purchased from Sigma-Aldrich (SaintLouis, USA). The dextran standards were purchased from Acmech Biochemical Co., Ltd. (Shanghai, China). The antibody p-I $\kappa$ B- $\alpha$ , I $\kappa$ B- $\alpha$ , p-IKK, p-JNK, p-38 were purchased from Cell Signaling Technology (Beverly, MA, USA). The antibody p-p65, p65, p-Akt, GAPDH,  $\beta$ -Tubulin were purchased from Affinity Biosciences LTD. (USA). NO assay kit, DAPI staining solution, Alexa Flour 488-labeled Goat Anti-Rabbit IgG (H + L) were purchased from Beyotime Institute of Biotechnology (Shanghai, China). The ROS assay kit was purchased from Elabscience Biotechnology Co. Ltd. (Wuhan, China). Dulbecco's modified eagle's medium (DMEM), fetal bovine serum (FBS) and streptomycin/penicillin were purchased from Gibco life technology (Waltham, MA, USA). All other reagents involved were analytically pure.

### 2.2. Extraction, isolation and purification of the exopolysaccharide

*P. distasonis* was cultured in BHI medium for 48 h at 37 °C under anaerobic condition. Then the seed solution was passaged twice with 3% inoculum. After that, the fermentation broth was collected for further study. The separation and purification methods were similar to previous studies (Zhai et al., 2021). In brief, the crude exopolysaccharide (named as PEP) was obtained by water extraction and alcohol precipitation, the protein in the polysaccharide was removed by papain and Sevag reagent, and the pigment was removed by AB-8 macroporous adsorption resin.

Then PEP solution was loaded onto DEAE cellulose DE-52 column (26 mm  $\times$  30 cm), and eluted stepwise with ultrapure water and different NaCl concentrations (0.1, 0.2, 0.3 and 0.5 M). Fraction was collected by determination of total sugar content using phenol-sulfuric acid method. The ultrapure water eluate was collected and lyophilized to obtain PEP-1. Then PEP-1 solution was subjected to Sephacryl S-300HR column (16 mm  $\times$  90 cm). The fraction detected by same method was harvested, dialyzed and lyophilized to obtain PEP-1A.

### 2.3. Determination of chemical composition

Total carbohydrate content of PEP-1A was assayed by phenol-sulfuric acid method with D-mannose as the standard (Liu et al., 2018). The protein content of PEP 1-A was mea-

sured using BCA protein assay kit (Beijing Cowin Biotech, China) with Bovine serum albumin as the reference.

#### 2.4. Determination of molecular weight

The homogeneity and molecular weight of PEP-1A was determined through HPGPC as a previous report (Zhang et al., 2017) with some modifications. PEP-1A solution (1 mg/mL) was analyzed using HPLC instrument (LC-20A, Shimadzu) equipped with an evaporative light-scattering detector (ELSD) and PolySep-GFC-P 4000 column (300 × 7.8 mm, Phenomenex). The mobile phase was ultrapure water at a flow rate of 1.0 mL/min. The drift tube temperature was 60 °C, and the gain value was 10. The column temperature was 35 °C and the injection volume was 20 µL. A linear curve was established by a series of dextran standards.

#### 2.5. Analysis of monosaccharide composition

The monosaccharide composition of PEP-1A was performed in the light of a previous method with slight modifications (Shen et al., 2017). In brief, 5.0 mg PEP-1A and 2 mL 3 M TFA solution were added to a sealed tube and were hydrolyzed at 120 °C for 6 h. The hydrolysate was rotated for several times with methanol to remove residual TFA. The residue, dissolved in deionized water, was treated with 100 µL 0.5 M PMP solution at 70 °C for 30 min in alkaline condition. After derivatization, 100 µL 0.3 M HCl solution and 200 µL deionized water were added to the reactant to neutralization and dilution. Then the resulting solution was treated with CHCl<sub>3</sub> for several times to remove extra PMP. Finally, the water layers were combined and passed through 0.45 µm filter membrane for HPLC analysis. A series of monosaccharide standards were derivatized in the same way and were finally analyzed by HPLC. 20 µL of solution was injected into a C<sub>18</sub> column (4.6 × 250 mm, 5 µm, Waters) and analyzed by HPLC instrument (LC-20A, Shimadzu) coupled with a diode array detector (DAD). The mobile phase was consisted of 0.05 M phosphate buffer (pH 6.7) and acetonitrile (83:17, v/v) at a flow rate of 1.0 mL/min. The detection wavelength was 250 nm.

#### 2.6. Methylation analysis

Methylation analysis of PEP-1A was carried out based on the reported method with minor revisions (Tian et al., 2021). Briefly, the vacuum-dried PEP-1A (6 mg) and 5 mL DMSO were added to a sealed tube and sonicated for 1 h at 18–20 °C, followed by adding 600 mg NaOH powder, then sonicated for another 1 h. Afterwards, the resulting solution was treated with 500 µL CH<sub>3</sub>I and sonicated for 10 min in the dark, the step was repeated three times. Then the reactant was added 4 mL ultrapure water to stop methylation, and 3 mL CHCl<sub>3</sub> was added to extract permethylated polysaccharide. After washing with ultrapure water for several times, the organic phase was rotated dried, and the residue, dissolved in 3 mL 3 M TFA, was hydrolyzed at 120 °C for 6 h. After removing the residual TFA by co-evaporation with methanol for three times, the residue was reduced by adding 2 mL ultrapure water and 20 mg NaBH<sub>4</sub> for 2 h at room temperature in the dark, and the glacial acetic acid was added to adjust pH to about

5.5 to terminate the reaction. Methanol was added several times to dry the reduction solution, and then the residue was treated with 2 mL acetic anhydride and pyridine at 95 °C for 1 h. After acetylation, the solution was dried and dissolved with 1 mL CHCl<sub>3</sub>. Finally, 1 µL of solution was analyzed after filtration using a GC-MS instrument (Trace DSQ II, Thermo Fisher Scientific) equipped with a TG-5SILMS column (30 m × 0.25 mm × 0.25 µm). The gas carrier was Helium with a flow rate of 1.0 mL/min. The inlet temperature was 250 °C, and the ion source temperature was 180 °C. The column temperature was increased from 100 °C to 250 °C at a rate of 3 °C/min, and kept at 250 °C for 5 min. The mass range was 40–400 *m/z*.

#### 2.7. UV, FT-IR and NMR spectrum analysis

PEP-1A solution (0.5 mg/mL in deionized water) was scanned from 200 nm to 400 nm on a UV-Vis spectrophotometer (UV-2600, Shimadzu, Japan).

FT-IR spectrum of PEP-1A was recorded on a Fourier transform-infrared spectrometer (Spectrum Two, PerkinElmer, USA) in the range of 4000–400 cm<sup>-1</sup> at a resolution of 4 cm<sup>-1</sup>.

35 mg PEP-1A was exchanged three times with D<sub>2</sub>O by repeated freezing and thawing, and then dissolved in 0.55 mL D<sub>2</sub>O. The <sup>1</sup>H NMR, <sup>13</sup>C NMR, COSY, HSQC, HMBC were recorded on a Cyroprobe 600 MHz spectrometer (Bruker BioSpin, Germany).

#### 2.8. Immunomodulatory activity of PEP-1A on RAW 264.7 cells

##### 2.8.1. Cell culture and treatments

The RAW 264.7 murine macrophage was grown in DMEM medium supplemented with 10% FBS and 1% penicillin-streptomycin at 37 °C in a humidified incubator containing 5% CO<sub>2</sub>.

The cells were incubated overnight to adhere before treatment. Briefly, the cells treated with LPS (1 µg/mL) were considered as positive controls; while cells without any other treatments were considered as negative controls.

##### 2.8.2. Cell viability assay

Cells were cultured in a 96-well plate at a density of 2 × 10<sup>4</sup> cells/well. After treatments with LPS (1 µg/mL), PEP-1A (10–100 µg/mL) and DMEM medium for 24 h, cells were observed and photographed on an inverted microscope (Nikon Eclipse Ts2, Japan). Then the subsequent operation was same as the previous report (Zhou et al., 2021). Finally, the absorbance of every well was measured at 490 nm using a microplate reader (Epoch 2, BioTek, USA).

##### 2.8.3. ROS assay

Cells were cultured in a 96-well plate at a density of 1 × 10<sup>5</sup> cells/well. After the same treatments as Section 2.8.2., ROS determination was followed by the previous method (Wu et al., 2020), while the fluorescence intensity of each well was examined using a fluorescence microplate reader (SpectraMax i3x, Molecular Devices, Austria) at excitation wavelength of 500 nm and emission wavelength of 525 nm.

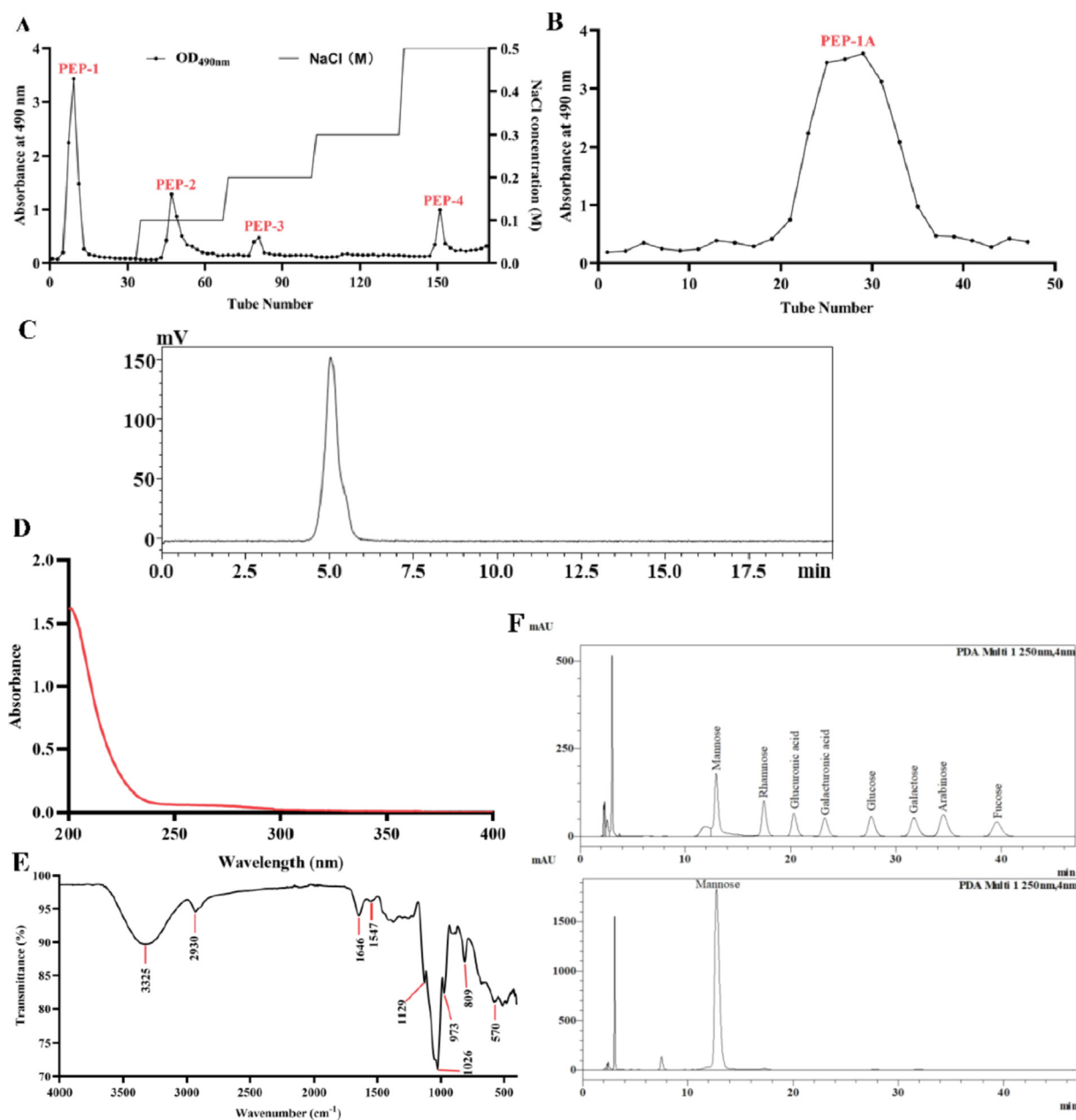


**Fig. 1** Purification and characterization of PEP-1A. Elution curve of PEP-1A by DEAE Cellulose DE-52 (A) and Sephacryl S-300HR (B). HPGPC (C), UV (D) and FT-IR spectrum (E) of PEP-1A. HPLC of standard monosaccharide and PEP-1A (F).

**Table 1** Glycosyl linkages analysis of PEP-1A based on GC-MS.

RT (min)	Methylated sugar	Mass fragments ( <i>m/z</i> )	Molar ratio	Type of linkage
28.64	2, 3, 4, 6-Me <sub>4</sub> -Manp	43, 71, 87, 101, 117, 129, 145, 161, 205	7.41	Manp-(1→
31.51	3, 4, 6-Me <sub>3</sub> -Manp	43, 87, 129, 161, 189	3.90	→2)-Manp-(1→
32.01	2, 4, 6-Me <sub>3</sub> -Manp	43, 71, 87, 99, 101, 117, 129, 161, 234	1.00	→3)-Manp-(1→
32.66	2, 3, 4-Me <sub>3</sub> -Manp	43, 87, 99, 101, 117, 161, 189	2.43	→6)-Manp-(1→
35.77	3, 6-Me <sub>2</sub> -Manp	43, 87, 99, 113, 129, 189, 233	6.17	→2, 4)-Manp-(1→
36.04	2, 4-Me <sub>2</sub> -Manp	43, 87, 117, 129, 189, 201, 233	0.36	→3, 6)-Manp-(1→
37.99	3-Me <sub>1</sub> -Manp	43, 87, 129, 189, 201, 261	0.24	→2, 4, 6)-Manp-(1→

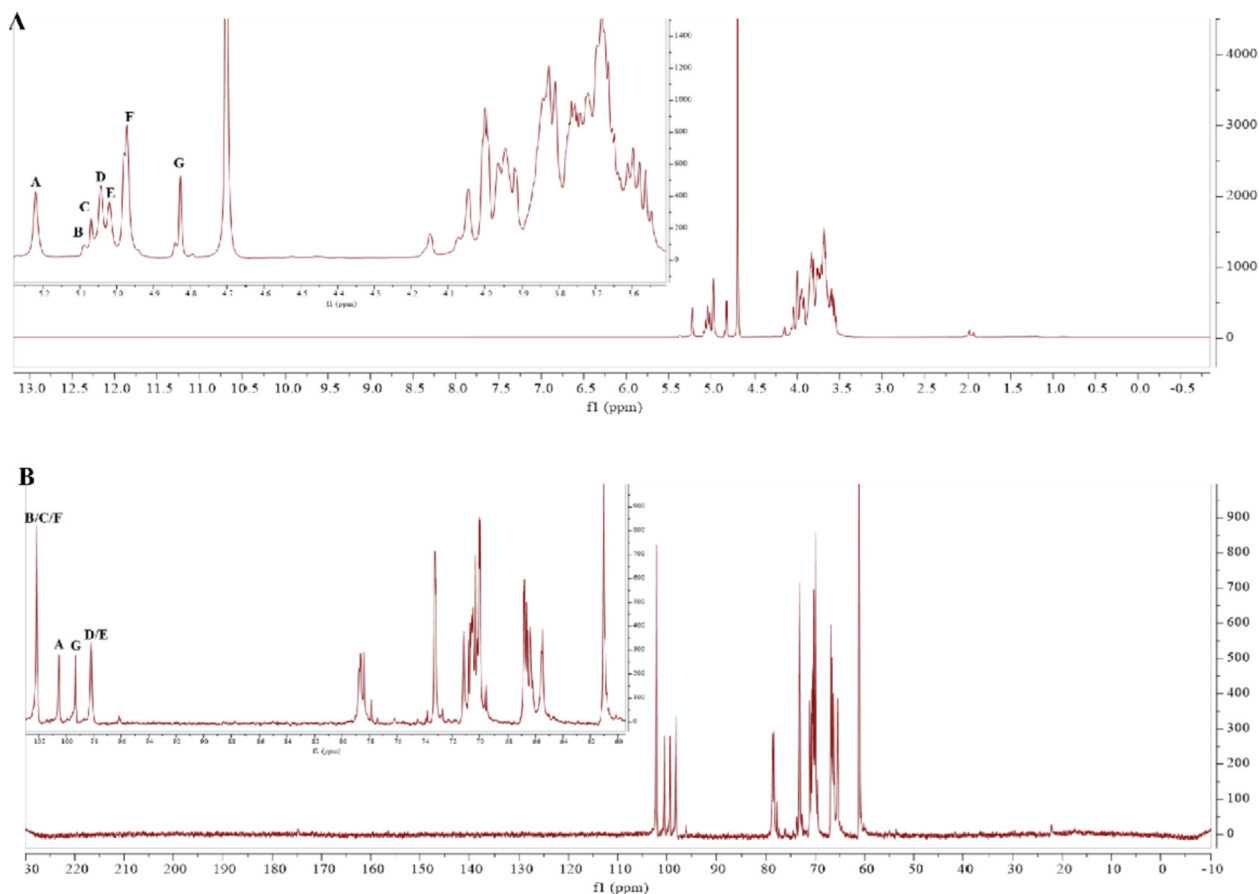


**Fig. 2** <sup>1</sup>H NMR spectrum (A) and <sup>13</sup>C NMR spectrum (B) of PEP-1A.

#### 2.8.4. NO assay

Cells were seeded in a 96-well plate at a density of  $2 \times 10^5$  cells/well. After the same treatments as Section 2.8.2., NO determination was same as the previous method (Wu et al., 2021), finally the optical density of each well was determined at 540 nm using a microplate reader.

The polymyxin B was employed to exclude the presence of endotoxin in PEP-1A. In brief, the cells were pre-treated with PMB (100 U/mL) for 1 h (Xu et al., 2018), then the cells were cultured with or without PEP-1A (100  $\mu$ g/mL) and LPS (1  $\mu$ g/mL) respectively for 24 h. Afterwards, the NO production was measured by Griess Reagent.

#### 2.8.5. Phagocytosis assay

Cells were seeded in a 96-well plate at a density of  $1 \times 10^5$  cells/well. After the same treatments as Section 2.8.2., neutral red determination was the same as previous method (You et al., 2020), eventually the absorbance of each well was recorded at 540 nm by a microplate reader.

#### 2.8.6. Determination of the mRNA expression of *IL-1 $\beta$* , *IL-6*, *TNF- $\alpha$* and *iNOS*

Cells were plated in a 6-well plate at a density of  $1 \times 10^6$  cells/well. After the same treatments as Section 2.8.2., the total RNA was extracted with Trizol reagent based on the instructions. Then, the RNA was reverse transcribed into cDNA using the Reverse transcription kit (TOYOBO Biotech, Japan) according to the protocol. The cDNA was amplified by using

the SYBR Real-time PCR kit (TOYOBO Biotech, Japan) on Real-time fluorescence quantitative PCR instrument (LightCycler 96, Roche, Switzerland). The sequence of each primer was shown in Table S1. GAPDH was served as the reference gene. The expression of mRNA was calculated by the  $2^{-\Delta\Delta C_t}$  method.

#### 2.8.7. Nuclear translocation of *p65*

Cells were seeded in confocal dishes at a density of  $1.5 \times 10^6$  cells/dish. After treated with LPS (1  $\mu$ g/mL), PEP-1A (100  $\mu$ g/mL) and DMEM medium for 6 h, the subsequent procedure was performed as previous literature (Wang et al., 2016). Eventually, cells were observed and photographed using a laser confocal microscope.

#### 2.8.8. Western blot

Cells were plated in a 6-well plate at a concentration of  $2 \times 10^6$  cells/well. After the same treatments as Section 2.8.2., the operations of protein extraction and western blot were the same as previous report (Qin et al., 2018). The membrane was blocked in BSA blocking solution for 2 h at room temperature with gentle shaking. Then, the membranes were incubated with primary antibody overnight at 4  $^{\circ}$ C. Afterwards the membranes were incubated with the corresponding secondary antibody for 2 h at room temperature with gentle shaking. The membranes were finally detected using ECL detection kit and photographed using Chem Studio 815 system (UVP, USA). Protein expression was analyzed by Image J (USA).

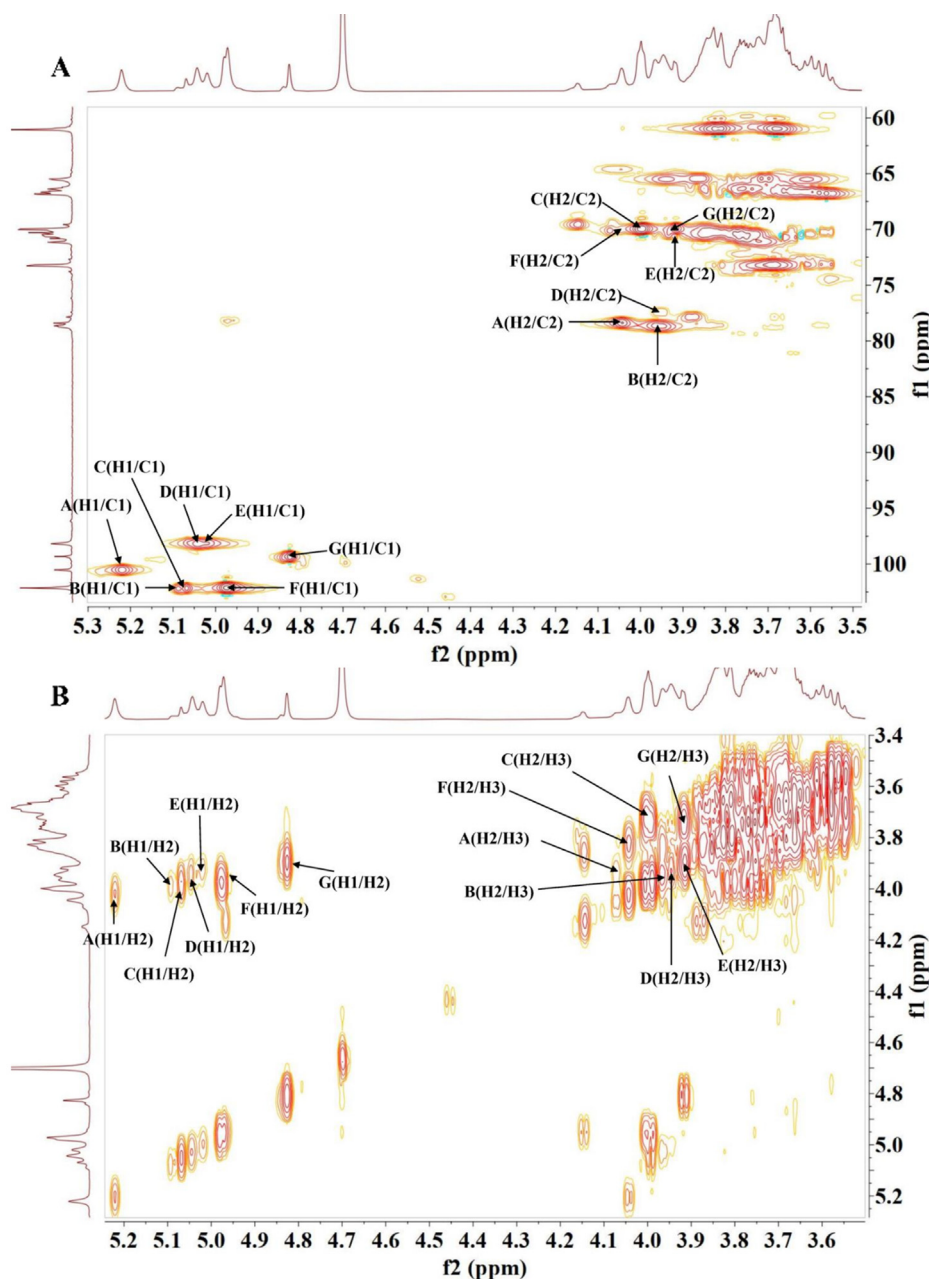


Fig. 3 HSQC (A) and COSY (B) spectrum of PEP-1A.

### 2.9. Statistical analysis

All of the tests were performed in triplicate. Data were expressed as mean  $\pm$  standard deviation (SD) and one-way ANOVA was used to analyze the significant differences between groups by SPSS 20 (IBM, USA). And  $p < 0.05$  showed significant difference.

## 3. Results

### 3.1. Purification and characterization of PEP-1A

The deproteinized and decolorized EPS were purified through column chromatography to obtain purified polysaccharides. As shown in Fig. 1A, four fractions were harvested by DEAE

Cellulose DE-52 separation, encoded as PEP-1, PEP-2, PEP-3 and PEP-4, respectively. The yield of PEP-1, PEP-2, PEP-3 and PEP-4 were 21.01%, 25.23%, 21.49% and 24.64%, respectively. PEP-1 was a fraction eluted from ultrapure water, indicating that PEP-1 was a neutral polysaccharide. On account of higher purity and better activity, PEP-1 was further purified by Sephacryl S-300HR column (Fig. 1B) to obtain the purity fraction, which was named as PEP-1A (yield of 54.74%). PEP-1A was subsequently analyzed for structural elucidation and immunomodulatory activity.

The total sugar content of PEP-1A was determined to be  $96.83\% \pm 1.12\%$ , and the protein content of PEP-1A was measured to be  $2.26\% \pm 0.76\%$ . HPGPC was used to analyze the molecular weight of PEP-1A. As shown in Fig. 1C, PEP-1A exhibited a single and sharp peak, which indicating the highly purity of PEP-1A. And the molecular weight of

Sugar residues		C1 H1	C2 H2	C3 H3	C4 H4	C5 H5	C6 H6/H6'
A	1,2- $\alpha$ -Manp	100.53	78.40	70.48	70.65	70.80	60.94
		5.22	4.05	3.84	3.75	3.70	3.74/3.83
B	1,2,4,6- $\alpha$ -Manp	102.14	78.79	70.15	77.82	70.47	66.57
		5.08	3.97	3.95	3.87	3.83	3.67/3.81
C	1,3,6- $\alpha$ -Manp	102.14	69.96	77.87	70.83	70.58	66.36
		5.07	4.00	3.68	3.65	3.72	3.77/3.84
D	1,2,4- $\alpha$ -Manp	98.18	78.66	70.65	77.82	73.29	60.82
		5.04	3.95	3.92	3.86	3.68	3.64/3.78
E	1,3- $\alpha$ -Manp	98.18	70.80	77.87	70.47	73.19	61.05
		5.02	3.92	3.87	3.81	3.66	3.68/3.75
F	1- $\alpha$ -Manp	102.14	70.00	71.16	70.59	71.16	60.67
		4.97	4.01	3.72	3.77	3.74	3.72/3.78
G	1,6- $\alpha$ -Manp	99.32	70.15	70.56	71.17	70.68	65.56
		4.83	3.92	3.74	3.72	3.77	3.73/3.86

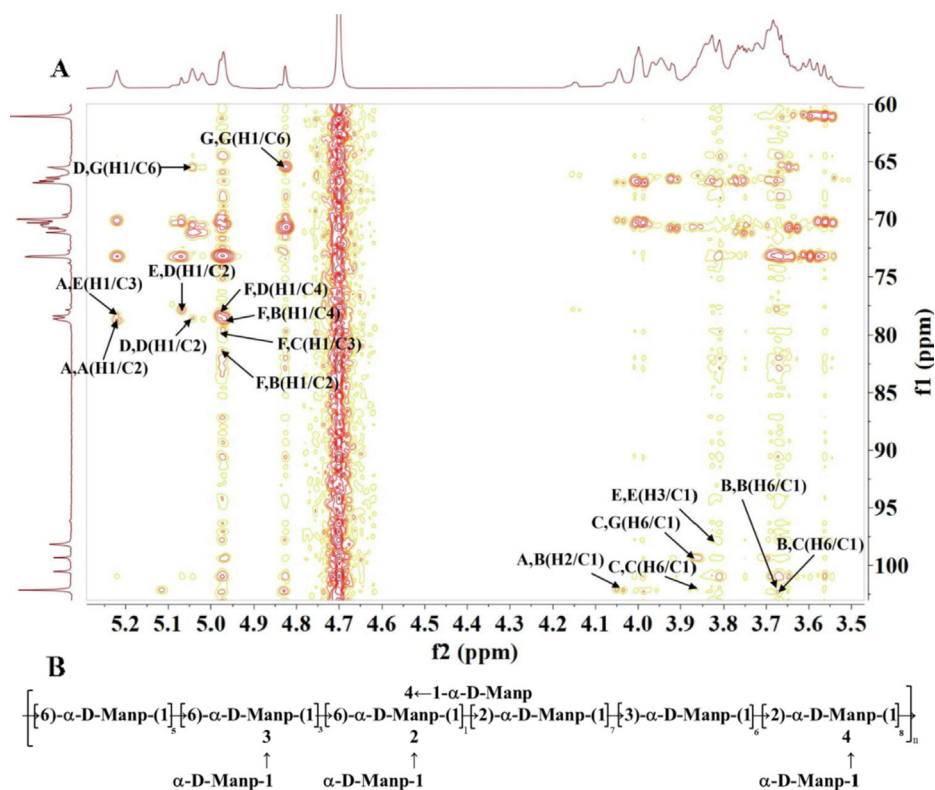


**Fig. 4** HMBC spectrum (A) and predicted structure (B) of PEP-1A.

PEP-1A was measured to be  $3.40 \times 10^6$  Da according to the standard curve.

UV spectroscopy was used to examine the purity of PEP-1A. As shown in Fig. 1D, no absorption at 260 nm and 280 nm indicated that PEP-1A contained little or no nucleic acid and protein, respectively.

FT-IR spectroscopy was an important auxiliary method to identify the functional groups in PEP-1A. As presented in Fig. 1E, the wide peak at  $3325 \text{ cm}^{-1}$  and the weak signal at  $2931 \text{ cm}^{-1}$  indicated the stretching vibration of O-H and

C-H, respectively. The absorption band at  $1646 \text{ cm}^{-1}$  indicated the presence of bound water (Cheng et al., 2020), and the weak absorption at  $1547 \text{ cm}^{-1}$  represented the trace amount of N-H bending of amide bonds of proteins (Wang et al., 2015), which was consistent with the result of protein content determination. The signals of  $1129 \text{ cm}^{-1}$ ,  $973 \text{ cm}^{-1}$  and  $1026 \text{ cm}^{-1}$  were attributed to pyranose ring (Zhang et al., 2022). The strong peaks at  $809 \text{ cm}^{-1}$  and  $570 \text{ cm}^{-1}$  were ascribed to  $\alpha$ -glycosidic linkage of mannose residue (Liu et al., 2018).

The HPLC chromatography (Fig. 1F) showed that PEP-1A was a homopolysaccharide, which was only consisted of mannose. The above result was in line with the result of  $809\text{ cm}^{-1}$  absorption in IR spectrum.

### 3.2. GC-MS analysis

Methylation analysis was a vital approach to distinguish the glycosidic linkage of PEP-1A. Complete methylation of PEP-1A was confirmed by the disappearance of O-H band ( $3000\text{--}3500\text{ cm}^{-1}$ ) in FT-IR spectrum (Fig. S1). The total ion chromatogram of GC-MS analysis was shown in Fig. S2A, and the mass spectrum of the fractions were illustrated in Fig. S2B-S5B. Seven sugar residues were found by comparing the ion fragments of partially methylated alditol acetates with the NIST database. The results of methylation on PEP-1A were summarized in Table 1. There were 1,5-Ac<sub>2</sub>-O-methyl-mannitol, 1,2,5-Ac<sub>3</sub>-O-methyl-mannitol, 1,3,5-Ac<sub>3</sub>-O-methyl-mannitol, 1,5,6-Ac<sub>3</sub>-O-methyl-mannitol, 1,2,4,5-Ac<sub>4</sub>-O-methyl-mannitol,

1,3,5,6-Ac<sub>4</sub>-O-methyl-mannitol, 1,2,4,5,6-Ac<sub>5</sub>-O-methyl-mannitol with a molar ratio of 7.41:3.90:1.00:2.43:6.17:0.36:0.24, which indicating that PEP-1A contained the glycosidic linkage of Manp-(1→, →2)-Manp-(1→, →3)-Manp-(1→, →6)-Manp-(1→, →2,4)-Manp-(1→, →3,6)-Manp-(1→, →2,4,6)-Manp-(1→). The total number of non-reducing ends was almost equal to the total number of branching residues, indicating that PEP-1A was completely methylated (Zhang et al., 2016).

### 3.3. 1D/2D NMR analysis

The <sup>1</sup>H NMR spectrum of PEP-1A was shown in Fig. 2A, seven anomeric protons at 5.22, 5.08, 5.07, 5.04, 5.02, 4.97 and 4.83 ppm in a ratio of nearly 7:1:3:8:6:13:5 were encoded A, B, C, D, E, F, G, respectively. No obvious peak in  $\delta$  5.40 ppm, which indicated that PEP-1A only contained pyranose (Xu et al., 2019). In <sup>13</sup>C NMR spectrum (Fig. 2B), four signals were found in the anomeric region at 102.15, 100.53, 99.33 and 98.17 ppm. The peaks at the  $\delta$  4.83–

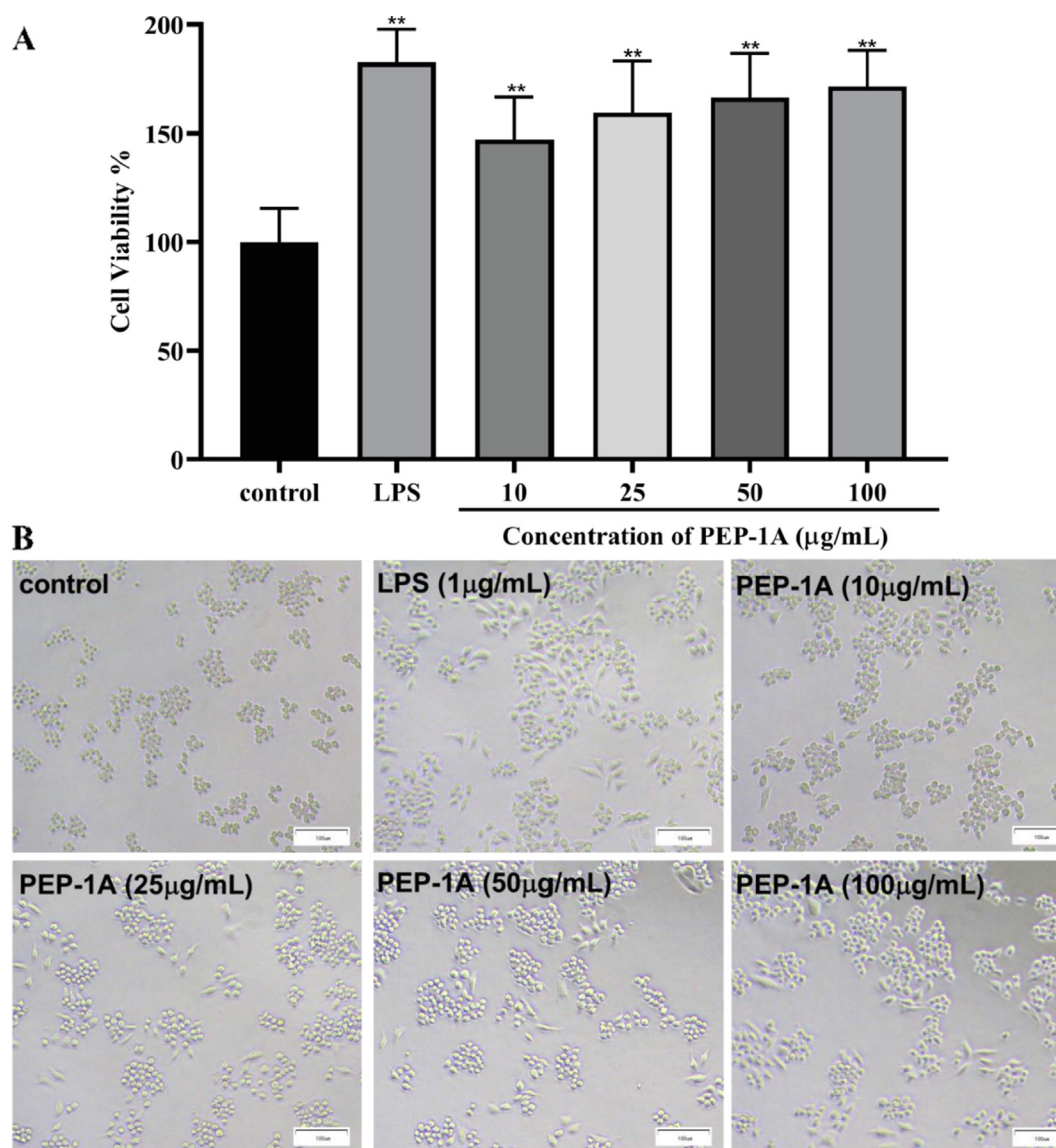


Fig. 5 Effect of PEP-1A on cell viability (A) and cell morphology (B). \* $p < 0.05$ , \*\* $p < 0.01$ .

5.22 ppm in  $^1\text{H}$  spectrum and the peaks at the  $\delta$  98-102 ppm in  $^{13}\text{C}$  spectrum, indicated that PEP-1A was mostly consisted of  $\alpha$ -configurations (Chatterjee et al., 2018; Yang et al., 2018; Zhang et al., 2019). From the HSQC spectrum (Fig. 3A), the anomeric carbon signals at 100.53 and 99.32 ppm were correlated to the anomeric proton signals  $\delta$  5.22 ppm (A),  $\delta$  4.83 ppm (G), respectively. However, the anomeric carbon signal at 102.14 ppm was correlated to the proton signals  $\delta$  5.08 ppm (B),  $\delta$  5.07 ppm (C) and  $\delta$  4.97 ppm (F), respectively. All the  $^1\text{H}$  and  $^{13}\text{C}$  signals were assigned (Table 2) using COSY and HSQC spectrum.

Residue A has an anomeric proton with a chemical shift at  $\delta$  5.22 ppm. The chemical shift of H-2 ( $\delta$  4.05 ppm), H-3 ( $\delta$  3.84 ppm), H-4 ( $\delta$  3.75 ppm), H-5 ( $\delta$  3.70 ppm), H-6 ( $\delta$  3.74,  $\delta$  3.83 ppm) were attributed on the basis of the COSY spectrum (Fig. 3B). The carbon signals from C-1 to C-6 were identified in the light of the HSQC spectrum, which were  $\delta$  100.53 ppm,  $\delta$  78.40 ppm,  $\delta$  70.48 ppm,  $\delta$  70.65 ppm,  $\delta$  70.80 ppm and  $\delta$  60.94 ppm, respectively. Compare with standard methyl mannitol (Agrawal, 1992), the downfield shifts of the C-2 ( $\delta$  78.40 ppm) carbon signal suggested that residue A was  $\rightarrow$  2)- $\alpha$ -D-Manp-(1 $\rightarrow$ .

Deduced in the same way, residue B, C, D, E, F, G were identified to be  $\rightarrow$  2, 4, 6)- $\alpha$ -D-Manp-(1 $\rightarrow$ ,  $\rightarrow$ 3, 6)- $\alpha$ -D-Manp-(1 $\rightarrow$ ,  $\rightarrow$ 2, 4)- $\alpha$ -D-Manp-(1 $\rightarrow$ ,  $\rightarrow$ 3)- $\alpha$ -D-Manp-(1 $\rightarrow$ ,  $\alpha$ -D-Manp-(1 $\rightarrow$ ,  $\rightarrow$ 6)- $\alpha$ -D-Manp-(1 $\rightarrow$ , respectively.

Monosaccharide residue binding site of PEP-1A were established according to the spectrum of HMBC (Fig. 4A). The

internal residue interactions were observed as following:  $\text{D}_{\text{H-1}}/\text{G}_{\text{C-6}}$ ,  $\text{F}_{\text{H-1}}/\text{D}_{\text{C-4}}$ ,  $\text{E}_{\text{H-1}}/\text{D}_{\text{C-2}}$ ,  $\text{B}_{\text{H-6}}/\text{C}_{\text{C-1}}$ ,  $\text{F}_{\text{H-1}}/\text{C}_{\text{C-3}}$ ,  $\text{A}_{\text{H-2}}/\text{B}_{\text{C-1}}$ ,  $\text{F}_{\text{H-1}}/\text{B}_{\text{C-2}}$ ,  $\text{F}_{\text{H-1}}/\text{B}_{\text{C-4}}$ ,  $\text{A}_{\text{H-1}}/\text{E}_{\text{C-3}}$ ,  $\text{A}_{\text{H-1}}/\text{A}_{\text{C-2}}$ ,  $\text{B}_{\text{H-6}}/\text{B}_{\text{C-1}}$ ,  $\text{C}_{\text{H-6}}/\text{C}_{\text{C-1}}$ ,  $\text{D}_{\text{H-1}}/\text{D}_{\text{C-2}}$ ,  $\text{E}_{\text{H-3}}/\text{E}_{\text{C-1}}$ ,  $\text{G}_{\text{H-1}}/\text{G}_{\text{C-6}}$ ,  $\text{C}_{\text{H-6}}/\text{G}_{\text{C-1}}$ . Eventually, combined with GC-MS results, the structure of PEP-1A was deduced in Fig. 4B, which showed that PEP-1A was a branched polysaccharide with multiple linkage patterns. In previous report, polysaccharides only containing mannose are rare. Marine bacterium *Edwardsiella tarda* was reported to produce a homopolysaccharide with mannose as a monomer containing both  $\alpha$ - and  $\beta$ -configurations (Guo et al., 2010). SSEPS2, a mannan isolated from *Sanghuangporus sanghuang*, was comprised of 1,3-, 1,2,6-, and 1,2-linked  $\alpha$ -D-Manp residues in the main skeleton, with the branches composed of  $\alpha$ -D-1,6-linked Manp residues, along with a terminal  $\alpha$ -D-Manp residue (Cheng et al., 2020). Mannan from yeast cell wall with good antioxidant activities, but its structure was unknown (Liu et al., 2018). In general, there are some differences between the structure of the above mannan and PEP-1A, indicating that PEP-1A was a novel polysaccharide.

#### 3.4. Effect of PEP-1A on cytotoxicity and morphology of RAW 264.7 cells

Before studying the immunostimulatory activity of PEP-1A, a MTT assay was performed to evaluate the cytotoxicity of PEP-1A on RAW 264.7 macrophage cells, and the cell viability of blank control was considered as 100%. As shown in

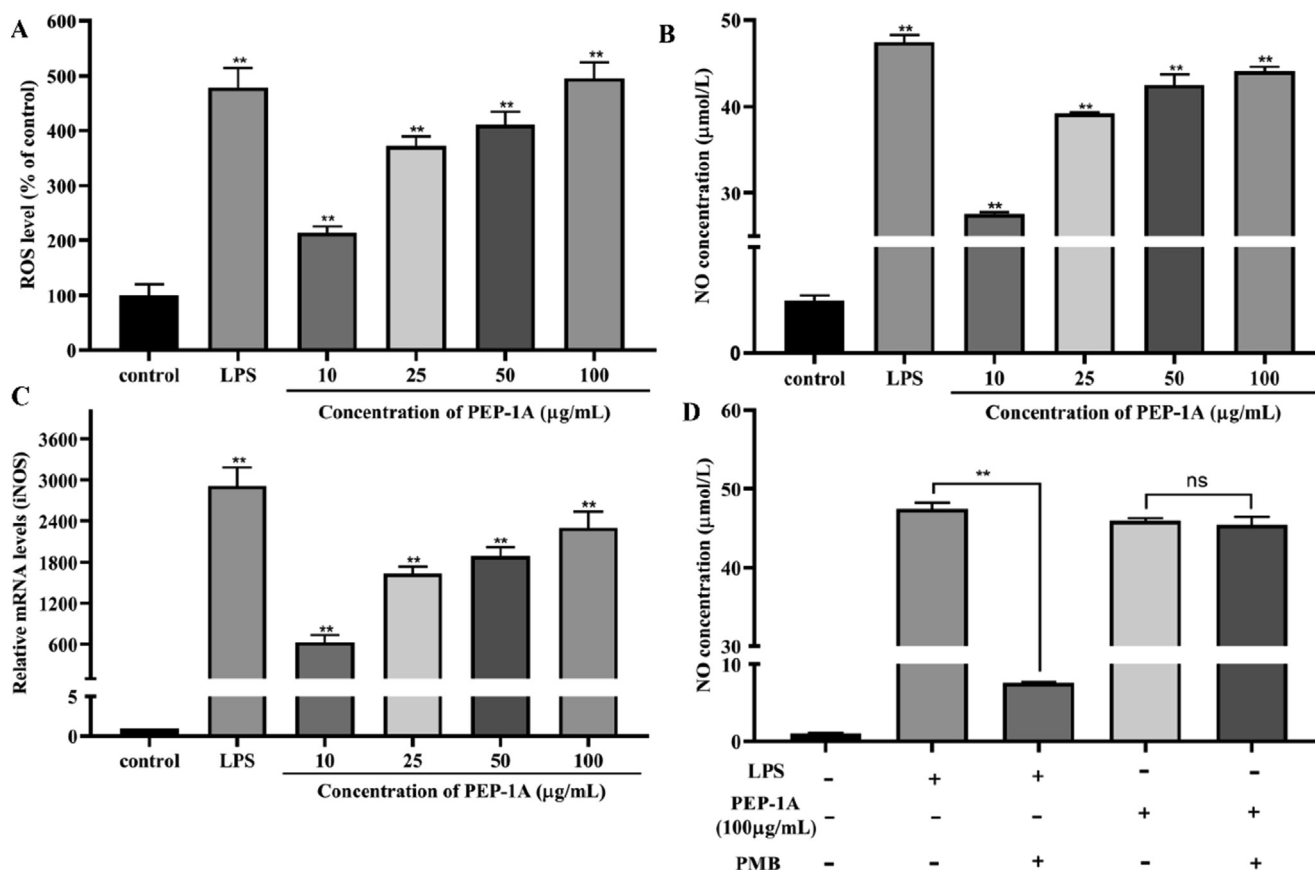


Fig. 6 Effect of PEP-1A on ROS production (A), NO production (B), relative mRNA expression of iNOS (C) and the effect of PMB on NO production (D). \*p < 0.05, \*\*p < 0.01, ns = no significance.

Fig. 5A, PEP-1A (10–100  $\mu\text{g}/\text{mL}$ ) stimulated the proliferation of RAW 264.7 cells in a concentration-dependent manner compared to the blank control group, indicating that PEP-1A was non-toxic to RAW 264.7 cells in the experimental concentrations.

Then we observed the morphology of RAW 264.7 cells after treatments, as shown in Fig. 5B, the cells in the control group were plump and round without pseudopod. While the cells stimulated by PEP-1A showed pseudopodia, and the cell volume was obviously enlarged and spindle shaped. Generally, morphological changes in RAW 264.7 cell indicated cellular activation, which made macrophages more capable of responding to invaders from pathogens (Wang et al., 2014). The result indicated that PEP-1A might activate the macrophages.

### 3.5. Effects of PEP-1A on ROS production of RAW 264.7 cells

Reactive oxygen species (ROS) play vital roles in host defense (Yu et al., 2014). DCFH-DA was used to determine the production of ROS. As presented in Fig. 6A, compared to control cells, the production of ROS was significantly increased after treatment with PEP-1A, indicating that PEP-1A motivated the generation of intracellular ROS.

### 3.6. Effects of PEP-1A on NO production and iNOS expression of RAW 264.7 cells

Nitric oxide (NO) is derived from L-arginine by catalysis of nitric oxide synthases (NOS). As an important intercellular signaling molecule, NO participates in plenty of immune responses to defense against pathogens (Wink et al., 2011). Herein we measured the NO production and the mRNA expression of iNOS. As shown in Fig. 6B and 6C, compared to the control cells, both the mRNA expression of iNOS and the NO production were observably increased in a dose-dependent manner after being stimulated by PEP-1A. The above results suggested that PEP-1A stimulation might promote the NO production by increasing the expression of iNOS thereby to exert the immunostimulatory activity in RAW 264.7 cells.

As shown in Fig. 6D, the presence or absence of PMB had no significant effect on NO production after stimulated by PEP-1A. While, NO production was sharply decreased when co-treated with LPS and PMB compared to treated LPS merely, indicating that the immunostimulatory activity of PEP-1A on RAW 264.7 cells had no concern with endotoxin.

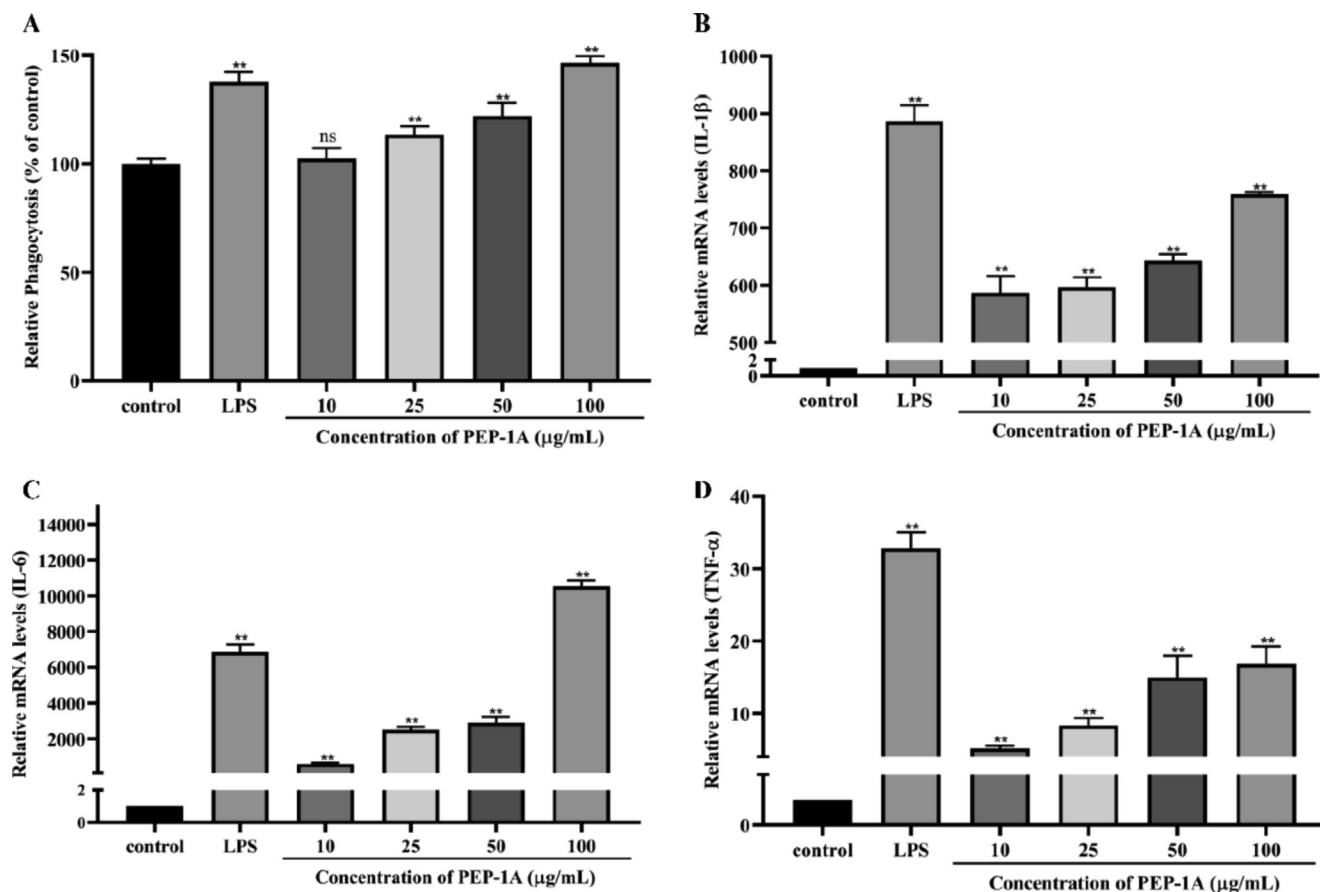


Fig. 7 Effect of PEP-1A on neutral red uptake (A), Relative mRNA expression of IL-1 $\beta$  (B), IL-6 (C) and TNF- $\alpha$  (D). \*p < 0.05, \*\*p < 0.01.

### 3.7. Effects of PEP-1A on phagocytosis of RAW 264.7 cells

Phagocytosis is the most critical process of macrophages to resist and clear pathogens (Gordon, 2016). The phagocytic activity of RAW 264.7 cells were firstly investigated by the uptake of neutral red. As shown in Fig. 7A, compared to the control cells, treatment with PEP-1A markedly increased the phagocytosis rate of neutral red in a concentration-dependent manner. The above results suggested that PEP-1A could improve the phagocytosis activity of RAW 264.7 cells so as to activate their corresponding immune response.

### 3.8. Effects of PEP-1A on IL-1 $\beta$ , IL-6, TNF- $\alpha$ expression of RAW 264.7 cells

Inflammatory cytokines like IL-1 $\beta$ , IL-6, TNF- $\alpha$  are an important type of cytokines expressed by macrophages after activation and are responsible for regulating the host immune response (Y. Wang et al., 2019). To further determine whether the immunostimulatory activity of PEP-1A could influence the production of cytokines, the mRNA expressions of IL-1 $\beta$ , IL-6, TNF- $\alpha$  were measured. As shown in Fig. 7B-7D, the

expression of IL-1 $\beta$  along with IL-6 and TNF- $\alpha$  had a dramatic increase in a dose-dependent manner after treatment with PEP-1A compared with control group. These results indicated that PEP-1A exerted the immunostimulatory effect by promoting the secretion of IL-1 $\beta$ , IL-6, TNF- $\alpha$ .

### 3.9. Signaling pathways of PEP-1A on RAW 264.7 cells

NF- $\kappa$ B is a heterodimer complexes consisted mainly of p65 and p50. When inactivation, p65 is combined with inhibitory protein I $\kappa$ B in the cytoplasm. After activation by a lot of inducers, like polysaccharides, the upstream I $\kappa$ B kinase (IKK) is activated and phosphorylated, afterwards the I $\kappa$ B proteins are phosphorylated and released from p65, subsequently p65 proteins become phosphorylated and translocate into the nucleus to activate transcription of a variety of genes (Oeckinghaus et al., 2011). NF- $\kappa$ B signaling pathway is thought to be relevant to the immunomodulation by regulating the expression of related genes in immune and inflammatory responses (Li and Verma, 2002). The nuclear translocation of p65 was investigated in PEP-1A-treated RAW 264.7 cells by laser confocal microscopy. As shown in Fig. 8, only few p65

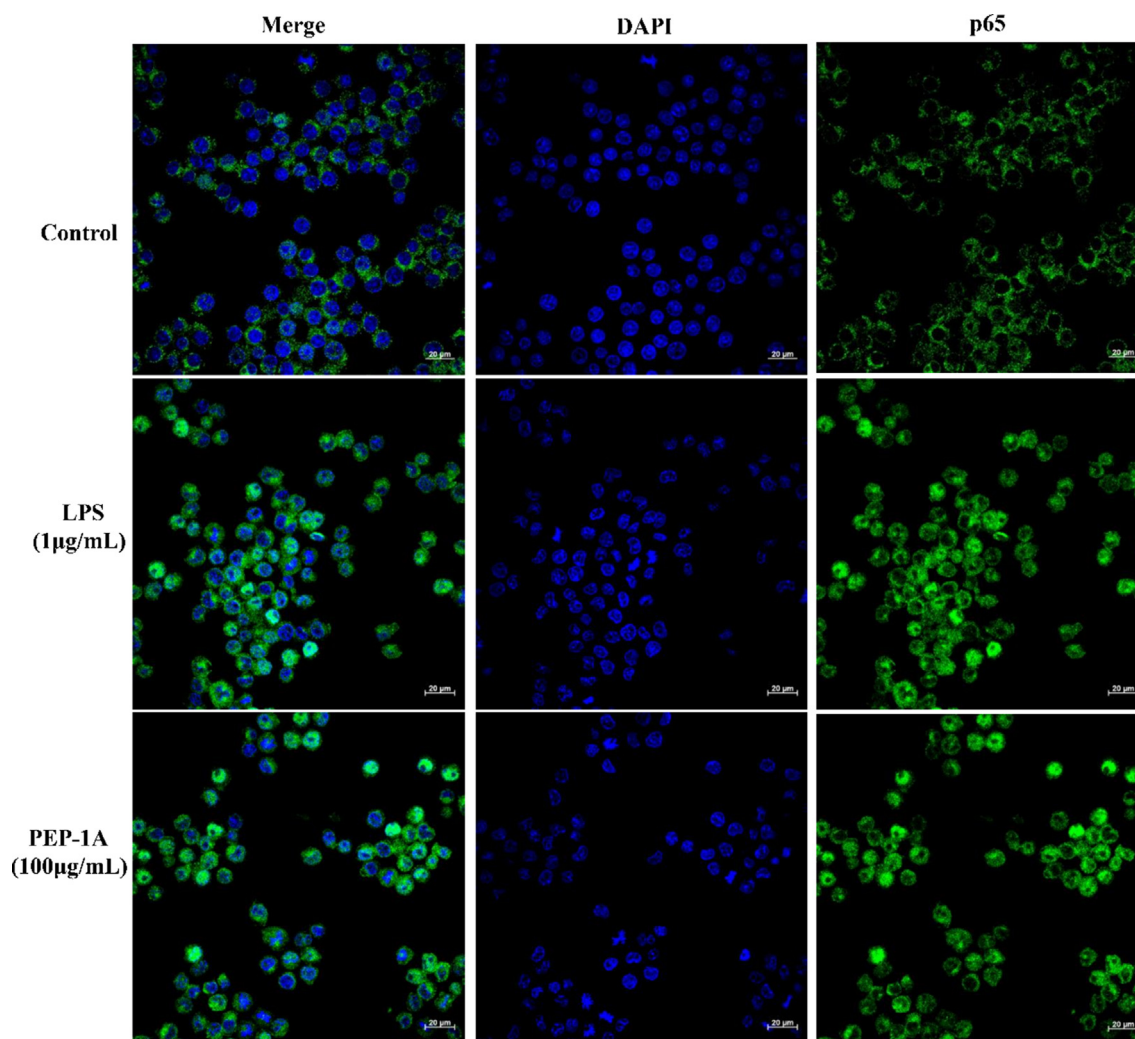


Fig. 8 Effect of PEP-1A on nuclear translocation of p65, scale label: 20  $\mu$ m.

was translocated to nucleus in control cells, however, obvious nuclear translocation of p65 was observed in PEP-1A-treated cells, along with LPS-treated cells, which revealed that PEP-1A induced the activation of macrophages by translocating the p65 to the nucleus. Furthermore, we investigated the expression of p65-related proteins using western blot assay. As shown in Fig. 9, PEP-1A stimulation could increase the phosphorylation of IKK, I $\kappa$ B- $\alpha$  and p65 on macrophages. These above results indicated that PEP-1A might enhance the immunomodulatory ability of macrophages by activating the NF- $\kappa$ B signaling pathway.

MAPK and Akt signaling pathways have been also thought to be vital to the proliferation, differentiation, survival and migration of macrophages (Fang and Richardson, 2005; Linton et al., 2019). We detected the proteins of MAPK (including ERK, JNK and p38) and Akt by Western blot. We found that PEP-1A could induced the phosphorylation of ERK, JNK, p38 and Akt in RAW 264.7 cells (Fig. 10), which suggested that Akt and MAPK signaling pathways were also involved in the immunoregulation of PEP-1A.

Combined with above results, it could be concluded that PEP-1A might activate macrophages based on NF- $\kappa$ B, MAPK and Akt signaling pathways to exert immunomodulatory activity. Meanwhile, we draw a schematic diagram (Fig. 11) to illustrate the possible mechanisms underlying the immunoregulatory activity of PEP-1A.

#### 4. Discussion

As biological response modifiers, EPS showed good immunomodulatory activity (Tian et al., 2021; Wang et al., 2021; Zhang et al., 2018). When the organism is in a state of immune deficiency such as infection or cancer, immunoregulation is crucial. Immunotherapy by improving immune function has also become one of the clinical methods to treat cancer (Elena Gonzalez-Guge et al., 2011). Considering that PEP-1A is also an EPS, we conjectured that PEP-1A has immune-enhancing effects similar to those of the polysaccharides mentioned above. Through experiments, we found that PEP-1A had the capacity to promote the phagocytosis, increase the production of ROS, NO, iNOS, IL-1 $\beta$ , IL-6, TNF- $\alpha$ , and to activate NF- $\kappa$ B, MAPK and Akt signaling pathway, and thus played an immunomodulatory role.

According to reports (Chatterjee et al., 2018; Cheng et al., 2020; Lakra et al., 2020; Liu et al., 2018), EPS containing only mannan is rare, and the structure of most mannans have not been identified, meanwhile the most literatures showing its activities are mainly antioxidant and anticancer. In this study, we isolated a mannan containing seven sugar residues from *P. distasonis* for the first time and demonstrated its immunomodulatory activity. The discovery of mannan could make up for the current scarcity of mannan. At the same time, as a novel mannan, the discovery of PEP-1A can broaden our

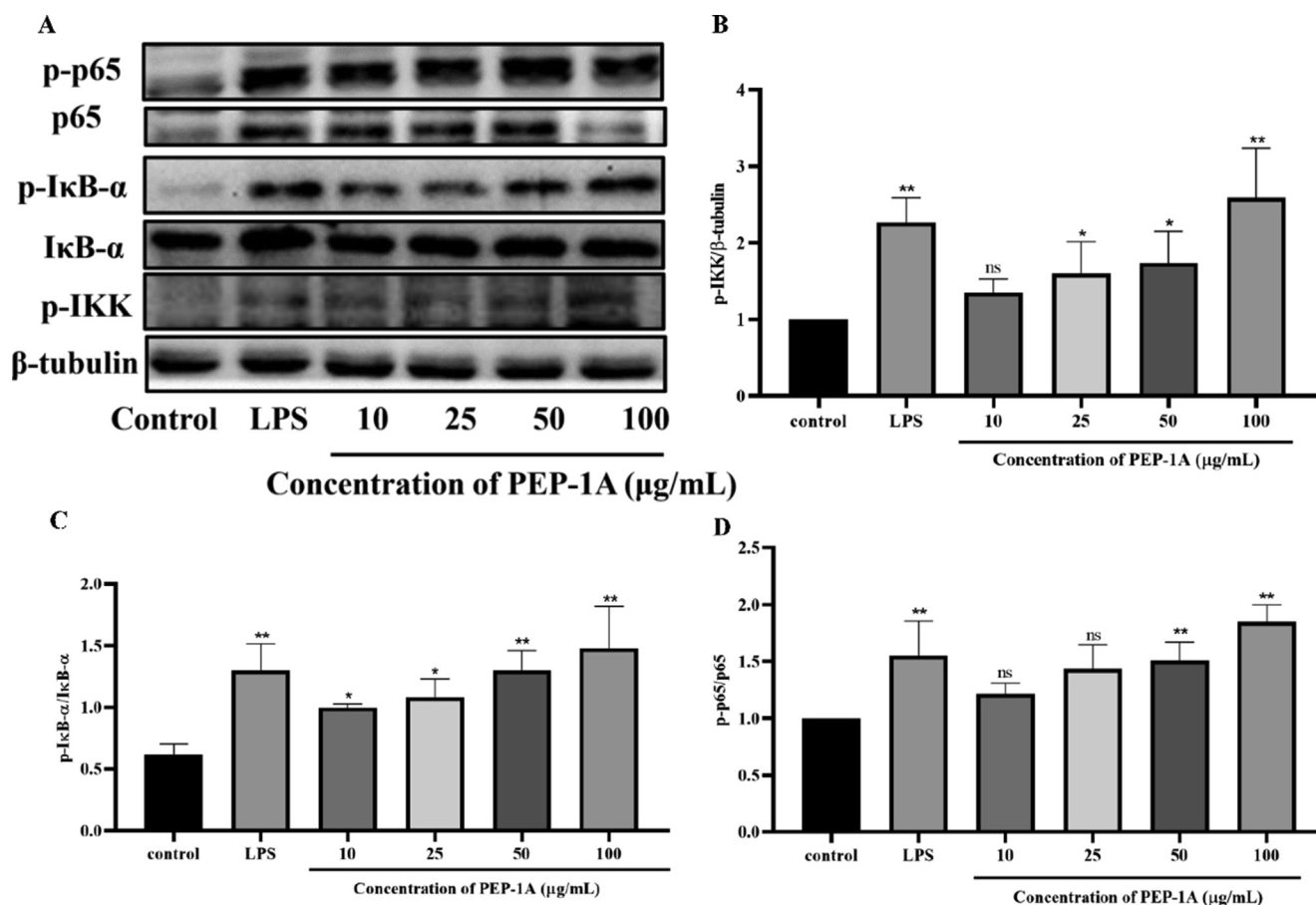


**Fig. 9** Effect of PEP-1A on NF- $\kappa$ B signaling pathway. Representative blot images (A). Protein expression of p-IKK (B), p-I $\kappa$ B- $\alpha$ /I $\kappa$ B- $\alpha$  (C) and p-p65/p65 (D). \* $p < 0.05$ , \*\* $p < 0.01$ , ns = no significance.

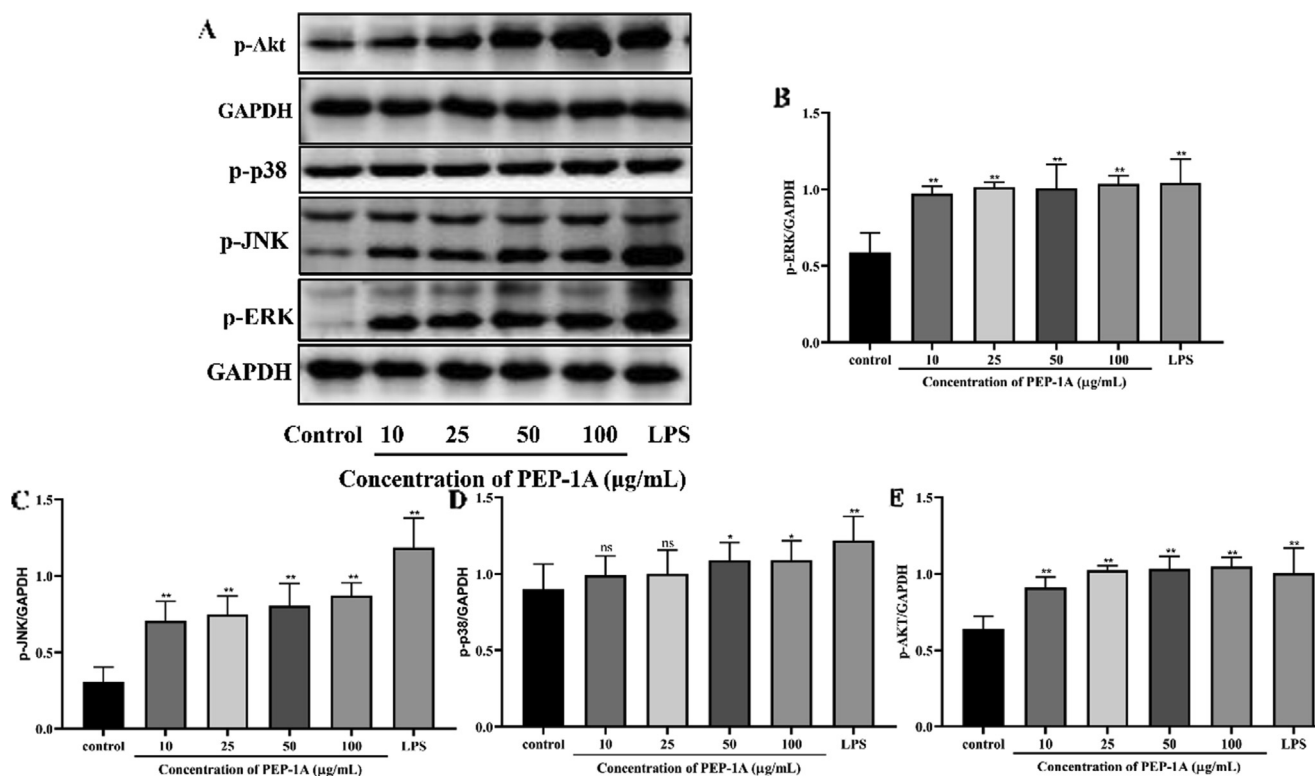


**Fig. 10** Effect of PEP-1A on MAPK and Akt signaling pathways. Representative blot images (A). Protein expression of p-ERK (B), p-JNK (C), p-38 (D) and p-Akt (E). \* $p < 0.05$ , \*\* $p < 0.01$ , ns = no significance.

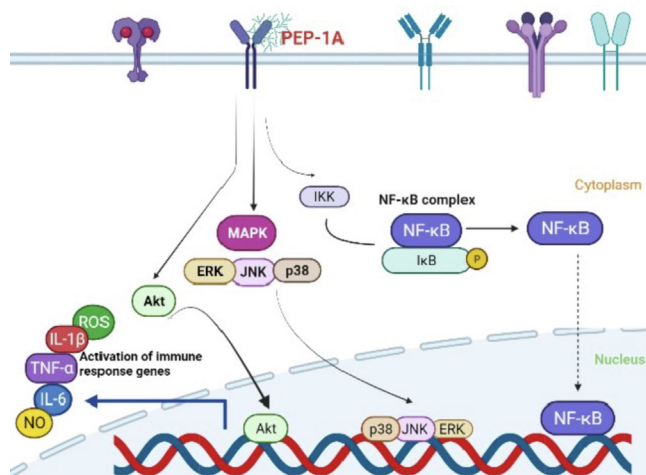


**Fig. 11** Possible signaling pathways related to the activation of macrophages by PEP-1A.

understanding of the structure and immunomodulatory activity of mannan.

Gut bacteria have their own unique behavior, presenting their health-promoting effects in the form of polysaccharides. *P. distasonis* is a probiotic gut strain with a variety of activities, meanwhile EPS is the metabolic by-product of *P. distasonis*. Therefore, it is possible to hypothesize that maybe we can discuss

the activity of intestinal bacteria including *P. distasonis* from the perspective of EPS in the future, so as to provide a new insight into the probiotic effect of intestinal bacteria, thereby more probiotic activities of intestinal bacteria can be explored.

Collectively, this is the first study to illuminate the detailed structure and immunomodulatory activity of PEP-1A from *P. distasonis*. The study lays a groundwork which PEP-1A will have potential application as a complementary drug for immunocompromised and immunodeficient populations, meanwhile further provides fresh perspective to discussed the gut microbiota with abundant probiotic effect.

## 5. Conclusions

In conclusion, a novel polysaccharide (PEP-1A) was extracted and purified from *P. distasonis*. PEP-1A had a backbone of  $\rightarrow 6$ - $\alpha$ -D-Manp-(1  $\rightarrow$  3, 6)- $\alpha$ -D-Manp-(1  $\rightarrow$  2, 4, 6)- $\alpha$ -D-Manp-(1  $\rightarrow$  2)- $\alpha$ -D-Manp-(1  $\rightarrow$  3)- $\alpha$ -D-Manp-(1  $\rightarrow$  2, 4)- $\alpha$ -D-Manp-(1  $\rightarrow$  with relatively high branching degree. Moreover, PEP-1A was found to have an immunomodulatory effect through enhancing the phagocytosis and increasing the secretion of ROS, NO, IL-1 $\beta$ , IL-6 and TNF- $\alpha$ , along with activating NF- $\kappa$ B, MAPK and Akt signaling pathways. This is the first time that we discovered and purified exopolysaccharide from *P. distasonis* with the potential as immunostimulant. The research not only paves a molecular foundation for the application of EPS, but also provides new insight into the probiotic mechanism of gut microbiota.

## CRedit authorship contribution statement

**Yanglu Zhu:** Investigation, Methodology, Writing – original draft. **Ying Cai:** Writing – review & editing, Validation. **Xueqin Cao:** Investigation, Validation. **Pei Li:** Conceptualization. **Deliang Liu:** Formal analysis. **Simin Ye:** Methodology. **Zengmei Xu:** Software. **Baochun Shen:** Visualization. **Qiongfeng Liao:** Supervision. **Hao Li:** Writing – review & editing. **Zhiyong Xie:** Resources, Data curation.

## Declaration of Competing Interest

The authors declare that they have no known competing financial interests or personal relationships that could have appeared to influence the work reported in this paper.

## Acknowledgements

This work was supported by the National Natural Science Foundation of China (No. U1803123, U1903211, 82174104, 22104158).

## Appendix A. Supplementary material

Supplementary data to this article can be found online at <https://doi.org/10.1016/j.arabjc.2022.103755>.

## References

- Agrawal, P.K., 1992. NMR Spectroscopy in the structural elucidation of oligosaccharides and glycosides. *Phytochemistry* 31, 3307–3330. [https://doi.org/10.1016/0031-9422\(92\)83678-R](https://doi.org/10.1016/0031-9422(92)83678-R).
- Cecanaviciute, E., Yoo, B.B., Runia, T.F., Debelius, J.W., Singh, S., Nelson, C.A., Kanner, R., Bencosme, Y., Lee, Y.K., Hauser, S.L., Crabtree-Hartman, E., Sand, I.K., Gacias, M., Zhu, Y., Casaccia, P., Cree, B.A.C., Knight, R., Mazmanian, S.K., Baranzini, S.E., 2017. Erratum: Gut bacteria from multiple sclerosis patients modulate human T cells and exacerbate symptoms in mouse models. *Proc. Natl. Acad. Sci. USA* 114, E8943. <https://doi.org/10.1073/pnas.1716911114>.
- Chatterjee, S., Mukhopadhyay, S.K., Gauri, S.S., Dey, S., 2018. Sphingobactan, a new  $\alpha$ -mannan exopolysaccharide from Arctic *Sphingobacterium* sp.  $\alpha$ ITKGP-BTPF3 capable of biological response modification. *Int. Immunopharmacol.* 60, 84–95. <https://doi.org/10.1016/j.intimp.2018.04.039>.
- Cheng, J., Song, J., Liu, Y., Lu, N., Wang, Y., Hu, C., He, L., Wei, H., Lv, G., Yang, S., Zhang, Z., 2020. Conformational properties and biological activities of  $\alpha$ -D-mannan from *Sanguangporus sanguang* in liquid culture. *Int. J. Biol. Macromol.* 164, 3568–3579. <https://doi.org/10.1016/j.ijbiomac.2020.08.112>.
- Dziarski, R., Park, S.Y., Kashyap, D.R., Dowd, S.E., Gupta, D., 2016. Pglyrp-Regulated gut microflora *Prevotella falsenii*, *Parabacteroides distasonis* and *Bacteroides eggerthii* enhance and *Alistipes finegoldii* attenuates colitis in mice. *PLoS ONE* 11, 1–24. <https://doi.org/10.1371/journal.pone.0146162>.
- Elena Gonzalez-Guge, Mansi Saxena, 2011. Modulation of innate immunity in the tumor microenvironment. *Cancer Immunol. Immunother.* 176, 139–148. <https://doi.org/10.1007/s00262-016-1859-9>.
- Fang, J.Y., Richardson, B.C., 2005. The MAPK signalling pathways and colorectal cancer. *Lancet Oncol.* 6, 322–327. [https://doi.org/10.1016/S1470-2045\(05\)70168-6](https://doi.org/10.1016/S1470-2045(05)70168-6).
- Farag, M.M.S., Moghannem, S.A.M., Shehabeldine, A.M., Azab, M. S., 2020. Antitumor effect of exopolysaccharide produced by *Bacillus mycoides*. *Microb. Pathog.* 140, 103947. <https://doi.org/10.1016/j.micpath.2019.103947>.
- Gordon, S., 2016. Phagocytosis: The Legacy of Metchnikoff. *Cell* 166, 1065–1068. <https://doi.org/10.1016/j.cell.2016.08.017>.
- Guo, S., Mao, W., Han, Y., Zhang, X., Yang, C., Chen, Y., Chen, Y., Xu, J., Li, H., Qi, X., Xu, J., 2010. Structural characteristics and antioxidant activities of the extracellular polysaccharides produced by marine bacterium *Edwardsiella tarda*. *Bioresour. Technol.* 101, 4729–4732. <https://doi.org/10.1016/j.biortech.2010.01.125>.
- Hidalgo-Cantabrana, C., Sánchez, B., Milani, C., Ventura, M., Margolles, A., Ruas-Madiedo, P., 2014. Genomic overview and biological functions of exopolysaccharide biosynthesis in *Bifidobacterium* spp. *Appl. Environ. Microbiol.* 80, 9–18. <https://doi.org/10.1128/AEM.02977-13>.
- Hotchkiss RS, Monneret G, P.D., 2013. Immunosuppression in sepsis: a novel understanding of the disorder and a new therapeutic approach. *Lancet Infect Dis.* 13, 260–268. [https://doi.org/10.1016/S1473-3099\(13\)70001-X](https://doi.org/10.1016/S1473-3099(13)70001-X).
- Hu, S.M., Zhou, J.M., Zhou, Q.Q., Li, P., Xie, Y.Y., Zhou, T., Gu, Q., 2021. Purification, characterization and biological activities of exopolysaccharides from *Lactobacillus rhamnosus* ZFM231 isolated from milk. *LWT-Food Sci. Technol.* 147, 111561. <https://doi.org/10.1016/j.lwt.2021.111561>.
- Jiang, B., Tian, L., Huang, X., Liu, Z., Jia, K., Wei, H., Tao, X., 2020. Characterization and antitumor activity of novel exopolysaccharide APS of *Lactobacillus plantarum* WLPL09 from human breast milk. *Int. J. Biol. Macromol.* 163, 985–995. <https://doi.org/10.1016/j.ijbiomac.2020.06.277>.
- Koh, G.Y., Kane, A. v., Wu, X., Crott, J.W., 2021. *Parabacteroides distasonis* attenuates tumorigenesis, modulates inflammatory markers and promotes intestinal barrier integrity in azoxymethane-treated A/J mice. *Carcinogenesis* 41, 909–917. <https://doi.org/10.1093/CARCIN/BGAA018>.
- Lakra, A.K., Domdi, L., Tilwani, Y.M., Arul, V., 2020. Physicochemical and functional characterization of mannan exopolysaccharide from *Weissella confusa* MD1 with bioactivities. *Int. J. Biol. Macromol.* 143, 797–805. <https://doi.org/10.1016/j.ijbiomac.2019.09.139>.
- Li, Q., Verma, I.M., 2002. NF- $\kappa$ B regulation in the immune system. *Nat. Rev. Immunol.* 2, 725–734. <https://doi.org/10.1038/nri910>.
- Linton, M.F., Moslehi, J.J., Babaev, V.R., 2019. Akt signaling in macrophage polarization, survival, and atherosclerosis. *Int. J. Mol. Sci.* 20. <https://doi.org/10.3390/ijms20112703>.
- Liu, Y., Huang, G., Lv, M., 2018. Extraction, characterization and antioxidant activities of mannan from yeast cell wall. *Int. J. Biol. Macromol.* 118, 952–956. <https://doi.org/10.1016/j.ijbiomac.2018.06.145>.
- Oeckinghaus, A., Hayden, M.S., Ghosh, S., 2011. Crosstalk in NF- $\kappa$ B signaling pathways. *Nat. Immunol.* 12, 695–708. <https://doi.org/10.1038/ni.2065>.
- Qin, D., Li, L., Li, J., Li, J., Zhao, D., Li, Y., Li, B., Zhang, X., 2018. A New Compound Isolated from the Reduced Ribose-Tryptophan Maillard Reaction Products Exhibits Distinct Anti-inflammatory Activity. *J. Agric. Food Chem.* 66, 6752–6761. <https://doi.org/10.1021/acs.jafc.8b01561>.
- Schepetkin, I.A., Quinn, M.T., 2006. Botanical polysaccharides: Macrophage immunomodulation and therapeutic potential. *Int. Immunopharmacol.* 6, 317–333. <https://doi.org/10.1016/j.intimp.2005.10.005>.
- Shen, Y., Wu, M., Xu, Z., Wan, Y., Zhang, L., Zhang, W., Xia, W., 2017. Structure elucidation and immunological activity of a novel glycopeptide from mannatide. *Int. J. Biol. Macromol.* 99, 112–120. <https://doi.org/10.1016/j.ijbiomac.2017.02.003>.
- Sun, H.Q., Yu, X.F., Li, T., Zhu, Z.Y., 2021. Structure and hypoglycemic activity of a novel exopolysaccharide of *Cordyceps militaris*. *Int. J. Biol. Macromol.* 166, 496–508. <https://doi.org/10.1016/j.ijbiomac.2020.10.207>.
- Tian, J., Zhang, C., Wang, X., Rui, X., Zhang, Q., Chen, X., Dong, M., Li, W., 2021. Structural characterization and immunomodulation

- latory activity of intracellular polysaccharide from the mycelium of *Paecilomyces cicadae* TJJ1213. *Food Res. Int.* 147. <https://doi.org/10.1016/j.foodres.2021.110515>.
- Wang, C., Cui, H., Wang, Y., Wang, Z., Li, Z., Chen, M., Li, F., 2014. Bidirectional immunomodulatory activities of polysaccharides purified from *Pleurotus nebrodensis*. *Inflammation* 37, 83–93. <https://doi.org/10.1007/s10753-013-9714-z>.
- Wang, G., Zhu, L., Yu, B., Chen, K.e., Liu, B., Liu, J., Qin, G., Liu, C., Liu, H., Chen, K., 2016. Exopolysaccharide from *Trichoderma pseudokoningii* induces macrophage activation. *Carbohydr. Polym.* 149, 112–120. <https://doi.org/10.1016/j.carbpol.2016.04.093>.
- Wang, J., Zhao, X., Yang, Y., Zhao, A., Yang, Z., 2015. Characterization and bioactivities of an exopolysaccharide produced by *Lactobacillus plantarum* YW32. *Int. J. Biol. Macromol.* 74, 119–126. <https://doi.org/10.1016/j.ijbiomac.2014.12.006>.
- Wang, K., Liao, M., Zhou, N., Bao, L., Ma, K., Zheng, Z., Wang, Y., Liu, C., Wang, W., Wang, J., Liu, S.J., Liu, H., 2019a. *Parabacteroides distasonis* Alleviates Obesity and Metabolic Dysfunctions via Production of Succinate and Secondary Bile Acids. *Cell Rep.* 26, 222–235.e5. <https://doi.org/10.1016/j.celrep.2018.12.028>.
- Wang, N., Jia, G., Wang, C., Chen, M., Xie, F., Nepovninnykh, N. v., Goff, H.D., Guo, Q., 2020. Structural characterisation and immunomodulatory activity of exopolysaccharides from liquid fermentation of *Monascus purpureus* (Hong Qu). *Food Hydrocoll.* 103. <https://doi.org/10.1016/j.foodhyd.2019.105636>
- Wang, Q.C., Wei, M., Zhang, J., Yue, Y., Wu, N., Geng, L., Sun, C., Zhang, Q., Wang, J., 2021. Structural characteristics and immune-enhancing activity of an extracellular polysaccharide produced by marine *Halomonas* sp. 2E1. *Int. J. Biol. Macromol.* 183, 1660–1668. <https://doi.org/10.1016/j.ijbiomac.2021.05.143>.
- Wang, Y., Zhang, Y., Shao, J., Ren, X., Jia, J., Li, B., 2019b. Study on the immunomodulatory activity of a novel polysaccharide from the lichen *Umbilicaria Esculenta*. *Int. J. Biol. Macromol.* 121, 846–851. <https://doi.org/10.1016/j.ijbiomac.2018.10.080>.
- Wink, D.A., Hines, H.B., Cheng, R.Y.S., Switzer, C.H., Flores-Santana, W., Vitek, M.P., Ridnour, L.A., Colton, C.A., 2011. Nitric oxide and redox mechanisms in the immune response. *J. Leukoc. Biol.* 89, 873–891. <https://doi.org/10.1189/jlb.1010550>.
- Wu, M., Feng, H., Song, J., Chen, L., Xu, Z., Xia, W., Zhang, W., 2020. Structural elucidation and immunomodulatory activity of a neutral polysaccharide from the Kushui Rose (*Rosa setata* x *Rosa rugosa*) waste. *Carbohydr. Polym.* 232, 115804. <https://doi.org/10.1016/j.carbpol.2019.115804>.
- Wu, M., Li, W., Zhang, Y., Shi, L., Xu, Z., Xia, W., Zhang, W., 2021. Structure characteristics, hypoglycemic and immunomodulatory activities of pectic polysaccharides from *Rosa setata* x *Rosa rugosa* waste. *Carbohydr. Polym.* 253, 117190. <https://doi.org/10.1016/j.carbpol.2020.117190>.
- Xu, Y., Cui, Y., Wang, X., Yue, F., Shan, Y., Liu, B., Zhou, Y., Yi, Y., Lü, X., 2019. Purification, characterization and bioactivity of exopolysaccharides produced by *Lactobacillus plantarum* KX041. *Int. J. Biol. Macromol.* 128, 480–492. <https://doi.org/10.1016/j.ijbiomac.2019.01.117>.
- Xu, Z., Yan, X., Song, Z., Li, W., Zhao, W., Ma, H., Du, J., Li, S., Zhang, D., 2018. Two heteropolysaccharides from *Isaria cicadae* *Miquel* differ in composition and potentially immunomodulatory activity. *Int. J. Biol. Macromol.* 117, 610–616. <https://doi.org/10.1016/j.ijbiomac.2018.05.164>.
- Yang, Y., Feng, F., Zhou, Q., Zhao, F., Du, R., Zhou, Z., Han, Y., 2018. Isolation, purification and characterization of exopolysaccharide produced by *Leuconostoc pseudomesenteroides* YF32 from soybean paste. *Int. J. Biol. Macromol.* 114, 529–535. <https://doi.org/10.1016/j.ijbiomac.2018.03.162>.
- You, X., Li, Z., Ma, K., Zhang, C., Chen, X., Wang, G., Yang, L., Dong, M., Rui, X., Zhang, Q., Li, W., 2020. Structural characterization and immunomodulatory activity of an exopolysaccharide produced by *Lactobacillus helveticus* LZ-R-5. *Carbohydr. Polym.* 235, 115977. <https://doi.org/10.1016/j.carbpol.2020.115977>.
- Yu, Q., Nie, S.P., Wang, J.Q., Yin, P.F., Huang, D.F., Li, W.J., Xie, M.Y., 2014. Toll-like receptor 4-mediated ROS signaling pathway involved in *Ganoderma atrum* polysaccharide-induced tumor necrosis factor- $\alpha$  secretion during macrophage activation. *Food Chem. Toxicol.* 66, 14–22. <https://doi.org/10.1016/j.fct.2014.01.018>.
- Zhai, Z., Chen, A., Zhou, H., Zhang, D., Du, X., Liu, Q., Wu, X., Cheng, J., Chen, L., Hu, F., Liu, Y., Su, P., 2021. Structural characterization and functional activity of an exopolysaccharide secreted by *Rhodospseudomonas palustris* GJ-22. *Int. J. Biol. Macromol.* 167, 160–168. <https://doi.org/10.1016/j.ijbiomac.2020.11.165>.
- Zhang, B., Lu, C., Xu, Z., Guo, H., Zhang, G., Hao, Y., 2022. Curculigo orchioides polysaccharides extraction, characterization, and their protective effects against femoral head necrosis. *Arab. J. Chem.* 15, 103414. <https://doi.org/10.1016/j.arabjc.2021.103414>.
- Zhang, G., Zhang, W., Sun, L., Sadiq, F.A., Yang, Y., Gao, J., Sang, Y., 2019. Preparation screening, production optimization and characterization of exopolysaccharides produced by *Lactobacillus sanfranciscensis* Ls-1001 isolated from Chinese traditional sourdough. *Int. J. Biol. Macromol.* 139, 1295–1303. <https://doi.org/10.1016/j.ijbiomac.2019.08.077>.
- Zhang, M., Wang, G., Lai, F., Wu, H., 2016. Structural Characterization and Immunomodulatory Activity of a Novel Polysaccharide from *Lepidium meyenii*. *J. Agric. Food Chem.* 64, 1921–1931. <https://doi.org/10.1021/acs.jafc.5b05610>.
- Zhang, M., Wu, W., Ren, Y., Li, X., Tang, Y., Min, T., Lai, F., Wu, H., 2017. Structural Characterization of a Novel Polysaccharide from *Lepidium meyenii* (Maca) and Analysis of Its Regulatory Function in Macrophage Polarization in Vitro. *J. Agric. Food Chem.* 65, 1146–1157. <https://doi.org/10.1021/acs.jafc.6b05218>.
- Zhang, Y., Zeng, Y., Men, Y., Zhang, J., Liu, H., Sun, Y., 2018. Structural characterization and immunomodulatory activity of exopolysaccharides from submerged culture of *Auricularia auricular-judae*. *Int. J. Biol. Macromol.* 115, 978–984. <https://doi.org/10.1016/j.ijbiomac.2018.04.145>.
- Zhao, D., Jiang, J., Liu, L., Wang, S., Ping, W., Ge, J., 2021. Characterization of exopolysaccharides produced by *Weissella confusa* XG-3 and their potential biotechnological applications. *Int. J. Biol. Macromol.* 178, 306–315. <https://doi.org/10.1016/j.ijbiomac.2021.02.182>.
- Zhou, T., Jiang, Y., Wen, L., Yang, B., 2021. Characterization of polysaccharide structure in *Citrus reticulata* ‘Chachi’ peel during storage and their bioactivity. *Carbohydr. Res.* 508, 108398. <https://doi.org/10.1016/j.carres.2021.108398>.